A UAV Infrared Measurement Approach for Defect Detection in Photovoltaic Plants

Pia Addabbo*, Antonio Angrisano*, Mario Luca Bernardi*
{p.addabbo, a.angrisano, m.bernardi}@unifortunato.eu

Graziano Gagliarde‡, Alberto Mennella‡, Marco Nisi§, Silvia Ullo †
{graziano.gagliarde,alberto.mennella}@topview.it, marco.nisi@grupposistematica.it, ullo@unisannio.it

*Giustino Fortunato University, Benevento, Italy
‡TopView S.r.l., Caserta, Italy
§Sistematica S.p.a., Terni, Italy
† University of Sannio, Benevento, Italy

***Abstract*—In the last two decades, the increased production and installation of photovoltaic (PV) plants worldwide has asked for efficient low-cost methods for PV plant inspection to monitor their functionality and guaranteed their performance. To lower maintenance costs new systems have been thought to substitute human workers inspecting the PV plants. The employment of Unmanned Aerial Vehicles (UAVs) has allowed realizing a fast detection of defects and problems arisen in PV plants thanks to the fusion of computer vision algorithms and high accuracy Global Navigation Satellite System (GNSS) positioning techniques able to detect and tag anomalies and identify the defective panels. Authors in this paper intend to present the state-of-the-art in the Computer Vision field applied to PV plant inspection and to thermal anomalies detection over the panels. In addition, different data sets have been recorded and compared for geo-referencing the solar panels. They have been derived through the U-blox NEO-M8N installed on board of the UAV used for inspection. Although the U-blox NEO-M8N measures are less accurate than the classic RTK GNSS ones, the measurements obtained with this handset introduce a very interesting novelty since initial services of the Galileo constellation, supported by the NEO-M8N GNSS module, have become available only since last December. Future testing and validation will be performed by using geo-referenced data from the RTK GNSS receiver, that has been ordered with a specially customized antenna whose specifications have been properly designed and sent to the manufacturer for its fabrication. Next campaigns will allow to get results also from this RTK receiver and to properly validate the proposed algorithm, by comparing new results with those found through the employment of U-blox receiver.**

***Index terms*—** Unmanned Aerial Vehicles (UAVs), photovoltaic (PV) plant inspection, image processing, Infrared (IR) measurements, GNSS receivers, geo-referencing

I. Introduction

Since 2000 annual production and installation of photovoltaic (PV) plants have grown hugely. PV market has moved from the 16.6 GW installed in more than 100 countries in 2010, to the 53 GW installed worldwide in 2015 and to an estimated value between 61 GW and 74 GW globally in 2016, of which 20 GW only in China [1], [2]. This considerable increase in the last two decades has been caused by a growing attention on climate issues and the consequent promotion of clean energy policies, with large amounts of incentives and funding made available in the specific sector by Governments and the European Economic Community itself. Also, after several years of relatively flat pricing, modules and components have begun a period of rapid price declines. The downward module price pressure has increased research on efficient techniques able to monitor PV plants and the failure of their components resulting into output power losses. A big concern of PV plant owners is, in fact, to rely on efficient maintenance procedures. Recognizing degradation and defects of PV cells is a very important issue to allow fast intervention and substitution of modules and cells to guarantee the PV plant performance. In recent years extended research has been conducted on automated remotely controlled systems for PV fields inspection, realized through the employment of Unmanned Aerial Vehicles (UAVs), to substitute human intervention and to ease the unavoidable huge activity of post-processing to finalize the data analysis. The employment of UAVs in PV plants monitoring can allow getting reliable information for the diagnosis of PV systems and presents several advantages: relatively low costs, fast detection, large area coverage, accuracy in defect detection through different sensors and cameras [3], [4], [5], [6]. Information acquired by UAVs is then transmitted to a remote console where subsequent interventions are activated by the detected anomalies. Maintenance companies are in this way equipped with tools useful to conduct an apriori analysis of the PV plant, which can be compared with the a-posteriori PV plant performance evaluation based on the final energy produced. The comparison of these data can help the maintainers to establish the value of investments in new maintenance and monitoring systems on the basis of the avoided losses and improved PV plant performance. Within the employment of UAVs for PV plant monitoring, a big step forward has been represented by the incorporation of Global Navigation Satellite System (GNSS) information to solve problems related to UAV accurate positioning and Panels geo-referencing over the PV plant. In this field of investigation, it stands the present work that has seen its first application in [7] where a low-cost GNSS (Global Navigation Satellite System) RTK (Real Time Kinematic) receiver has been mounted on board of a UAV system for locating the defective cell to be replaced. In this paper authors aim to improve some critical aspects related to the key tasks of direct geo-referencing, image acquisition, panel recognition and faulty module detection, and besides, they will present the interesting results come out of a validation campaign performed taking into account different datasets.

The paper is organized as follows: in the next Section II, the

978-1-5090-4234-0/17/$31.00 ©2017 IEEE

overall architecture is presented for the chosen UAV, to which we will refer generically as the Remotely Piloted Aircraft System (RPAS). The subsections describe respectively:

- The Payload Description and Specifications;
- The Geo-referencing issues;
- The Image Acquisition system.

In Section III the Experimental Setup is explained in detail with operations accomplished for data acquisition and the procedure used for classification. Obtained results are also presented and discussed. In Section IV conclusions and future work are discussed.

II. The Remotely Piloted Aircraft System (RPAS)

The model of proposed system Architecture is represented in Figure 1 where a UAV performs a mission flying over a photovoltaic field to collect optical and thermal images of solar panels in a PV plant. The data gathered by the UAV are processed through a computer vision algorithm running on-board the vehicle in tight synergy with a geo-software module, capable of tagging thermographic images using fixed centimeter-level positions provided by the commercial U-blox M8 series receivers. The accurate positioning provided by GNSS signals enables the automation of the entire process allowing to correctly geo-referencing the defective panel inspected by the thermal camera on-board the UAV. Finally, this information is provided to the remote service center in charge of defect identification and PV plant management. We refer to the overall architecture as Easy-PV Remotely Piloted Aircraft System (RPAS) Architecture, since the work presented in this paper is part of the ongoing activities performed in the framework of EASY-PV project sanctioned under H2020-Galileo-2015-1 call.
In order to highlight the originality of the contribution that the new paper intends to present with respect to the state of the art we underline the main differences in the following subsections.

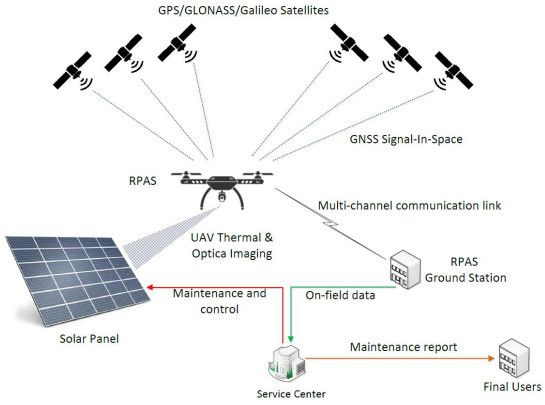

Figure 1: Easy-PV RPAS Architecture model

A. The Payload Description and Specifications

In Figure 1 the Architecture of the entire Easy-PV RPAS is represented. The Payload designed for this specific application exploits different Commercial Off-The-Shelf (COTS) available on the market and in particular:

- FLIR TAU2 640x512 14bit thermal camera
- DJI Zenmuse X3 optical camera and gimbal
- Intel Joule 570X quad-core as OBC (On-Board Computer)

However, a strong effort has been spent to design the specific I/F HW board required to command and control the thermal sensor and all the mechanism to keep it aligned for optimal nadiral acquisition during RPAS movements, and to keep the pointing error as low as possible. The heart of the payload is represented by the OBC element that has in charge different tasks such as:

- Handling sensors acquisitions
- Handling commands for payload control from pilot or payload operator
- Storing thermal and optical images acquired
- Hosting and handling computer vision algorithm
- Hosting and handling GEO-Tagging SW module
- Managing acquired data towards the Service Center

In Figure 2 a block diagram of the implemented payload is presented. The grey blocks represent the hardware modules of the payload; the yellow blocks represent the main software components.

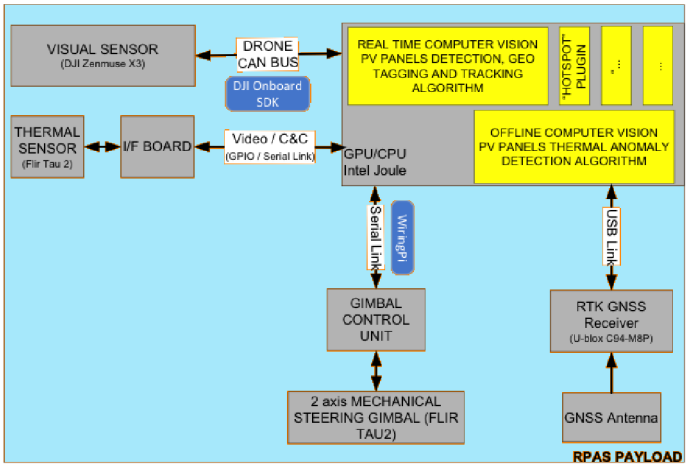

Figure 2: RPAS Payload block diagram

The optical and thermal images acquired are geo-tagged with a precise position information obtained from GNSS U-blox C94-M8P Receiver. The position (referred to the center of the antenna) is shifted, through a rotation matrix, to the thermal camera optical center. Such information is used by the OBC element to tag each image center with accurate geographical references.
The computer vision block has embedded PV Panel shape recognition features, while thermal anomalies typologies are handled as “plugin”. Such information is available to the pilot (or payload operator) as screen overlay in real time to add additional remarks to each panel (identified or not) in the case of need. For instance, in the case of algorithm bad identification of PV panels or in the case of false positives, the pilot (or payload operator) may flag suspect panels during flight operations, through his remote control screen. Such information is useful in after-flight post-processing to allow the second (offline) part of the algorithm to refine on the flagged

thermographies before the generation of the final XML stream to be sent to the service center.

B. The Geo-referencing issues

Global Navigation Satellite Systems (GNSSs) are satellite-based systems able to provide tridimensional position and synchronization to Universal Time Coordinates (UTCs); GPS is the most widespread GNSS, but several similar systems are currently available, e.g. the Russian Glonass, the European Galileo, the Chinese BeiDou. Absolute or Single Point Positioning (SPP) is the fundamental GNSS operational mode and it is based on the pseudorange equation [8]:

$$\rho = d + cdt_u + cdt_s + \Delta d_o + \Delta d_i + \Delta d_t + \Delta d_{mp} + \Delta d_n + \varepsilon \quad (1)$$

where:

- ρ is the pseudo range measurement, defined as the measured range between receiver and satellite,
- d is geometric distance between receiver and satellite,
- cdt_u and cdt_s are respectively the receiver and satellite clock offsets scaled by the speed of light,
- Δd_o is the orbital error,
- Δd_i and Δd_t are respectively the ionospheric and tropospheric delays,
- Δd_{mp} is the multipath error,
- Δd_n is the error related to receiver noise,
- ε includes the unmodelled errors.

The SPP mode has an accuracy of about 5-10 meters [9] and so it is usable in applications where requirements as mapping or precision farming are not so stringent. A typical approach to overcome this SPP limit is the differential mode, which makes use of one or more reference stations, placed in known surveyed positions around the GNSS receiver with unknown coordinates (at maximum 100 km). Differential mode, simply called DGNSS (Differential GNSS), is based on the spatial correlation of several measurement error sources, since errors in the reference station's measurements are expected to be very similar to those experienced by a nearby user. The pseudorange error sources cdt_s, Δd_o, Δd_i, Δd_t are spatially correlated and in the differential mode they are cancelled or strongly reduced, while the remaining error sources are not spatially correlated, and therefore they are not reduced or cancelled in the differential mode. In the open-sky, where drones typically operate, the main errors are related to the ionosphere, so in this scenario the DGNSS mode is very effective in reducing the error sources, improving the accuracy to 1-2 meters [9]. To obtain a centimeter level positioning, the carrier-phase measurement should be used along with pseudorange one. The most common technique using a carrier-phase measurement is the Real Time Kinematic (RTK), which exploits the differential concept too. The application considered herein, i.e. identification of defective photovoltaic panels by drones equipped with a thermal camera, requires a very accurate kinematic positioning, which currently can be obtained, in GNSS context, only using a RTK technique. In this work, the RTK receiver was not available from the beginning, so a DGNSS approach has been initially followed. Since the adopted GNSS device is unable to provide raw measurements, a position-domain DGNSS, based on NMEA information, has been implemented [10]. In the proposed algorithm, the only data necessary from the rover are GGA and GSA NMEA messages, while raw data are required from the reference station. GGA NMEA message contains the SPP coordinates of the rover, while GSA message contains the identifiers of the satellites used for the solution. The corrections computed at the reference station, called $\mathbf{d}\rho$, are projected on position domain using the design matrix, as shown below:

$$\mathbf{dx} = (H^T H)^{-1} H^T \mathbf{d}\rho \quad (2)$$

The design matrix H is expressed in local frame and results dependent on satellite elevation and azimuth coordinates.

C. The Image Acquisition System: PV module identification and defect detection

The Image Acquisition procedure is based on a very precise processing system that receives images from the thermal camera in input and produces final outputs through the proposed Computer Vision Algorithm. As already highlighted geo-referencing operations are crucial since precision is the pre-condition of a correct and successful data processing for the entire system. Thus, it is necessary, at the moment, the utilization of the DGPS technique which compensates the little accuracy of the present receiver, mounting on board the U-blox NEO-M8N. As above highlighted, although the U-blox NEO-M8N measures are less accurate, the measurements obtained with this handset introduce a very interesting novelty since initial services of the Galileo constellation, supported by the NEO-M8N GNSS module, have become available only since last December. Moreover DGNSS as already explained can compensate many of the error sources by ymproving accuracy.

The core of the Image Acquisition System is the Computer Vision Algorithm. It performs both PV module identification and defect detection and gives a unique ID for each panel and a precise relative position of defects in the metadata. Particularly, we are interested in finding PV defectiveness and PV failure, defined as an effect that results in safety or power loss for a PV module [11], [12]. The causes of defects in the PV panels can be damages occurred during the planning, the transportation and the installation stages, wich could produce, for example, glass breakage, with a consequent loss of PV performance, or effects of adverse environmental impacts. Among the main measurements methods used to identify PV defects, infrared imaging represents one of the most diffused techniques first of all because it is a non-invasive method for detection of thermal anomalies due to failures in PV modules, and secondly because this technique has reached very high levels of performance in defect detection with respect to other methodologies. Infrared imaging is suitable to detect many defects on PV plants, such as faults in bypass diodes, mechanically damaged cells, hot spots and fault contact points, that represent the main PV plant defect typologies [13].

In this work, the proposed Computer Vision Algorithm is based on the template matching technique, a high-level machine vision procedure for identification of the parts on an image that match a predefined template [14]. The algorithm is implemented using the OpenCV library, an open source project that started in 1999 by the computer-vision community [15], and it uses a Normalized Cross Correlation as a similarity measure for template matching [16].

III. Experimental Setup and Results

As already mentioned above, the images captured by the on-board thermal camera need an accurate positioning to enable the automation of the entire process allowing to correctly geo-referencing the defective panel. Images have to be tagged by means of fixed positions provided by the GNSS receiver. At the beginning the use of a RTK receiver was scheduled for the collection of geo-referenced data. Unfortunately, when employed it presented electromagnetic interference problems with the devices on board the UAV due to the magnet of which the RTK antenna is provided. For this reason, it has been ordered a specially customized antenna whose specifications have been properly designed and sent to the manufacturer for its fabrication. Meanwhile, it has been decided to begin data acquisition through the use of the U-blox NEO-M8N GNSS receiver in conjunction with the Differential GNSS mode. In the considered test, to perform DGNSS, a reference station placed at San Nicola la Strada (Caserta) and far few kilometres from the rover has been used. The chosen reference station belongs to the GNSS Campania Network and it is able to receive both GPS and Glonass measurements.

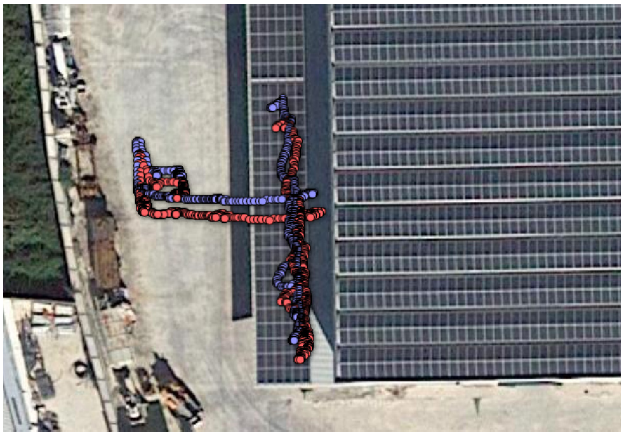

Figure 3: An example of flight on the area under test with and without differential correction - (•) DGPS (•) SPP

The dataset used for this work consists of a series of flights on a test site in Lo Uttaro, a location in the Province of Caserta, Italy. The UAV was flown over the test site with the manually navigated DJI Matrice 100 flight platform carrying on board a Thermal Camera Flir Vue Pro for thermal images acquisition in the 7.5 – 13.5 μm spectral band. In Figure 3 it is shown a flight on the area used for the test: the SPP positions extracted from NMEA file are depicted with red dots while the DGPS positions with blue ones.

In Figure 4, results of the proposed computer vision algorithm are shown, where a series of six consecutive images are analyzed. Black boxes with a G-number ID are used to identify panels on the PV plant. The panels that are totally contained in the images are correctly and uniquely identified as shown in the first row of images in Figure 4, while some panels are missing in the other case, shown in the second row of the same Figure. Blue boxes with a B-number ID are used to identify defects on the PV plant panels. Two true heating points (IDs: B5 and B13) are correctly detected, even if of different dimensions, and the false positive (ID: B15) present in both (a) and (b), is then corrected in the subsequent shot (c).

Three metrics have been defined and used to evaluate the classification results: Precision, Recall and F-Measure.

The precision has been computed as the proportion of the examples that truly belong to a specific class among all those which were assigned to that class. It is the ratio of the number of correct items that are detected by the total number of irrelevant and relevant items detected:

$$Precision = \frac{tp}{tp + fp} \tag{3}$$

where tp indicates the number of true positives and fp indicates the number of false positives.

The recall has been computed as the proportion of items that were assigned to a specific class, among all the items that truly belong to that class, i.e., how much the class has been covered. It is the ratio of the number of relevant items detected to the total number of relevant items in the search space:

$$Recall = \frac{tp}{tp + fn} \tag{4}$$

where fn indicates the number of false negatives.

The F-Measure is a measure of test accuracy, interpreted as a weighted average of the Precision and the Recall parameters above specified:

$$F\text{-}Measure = 2 * \frac{Precision * Recall}{Precision + Recall} \tag{5}$$

We have evaluated the effectiveness of the classification method with the procedure summarized below:

1) build a testing set T (gold standard) in which modules are identified and classified by an expert as ”Good” or ”Bad”;
2) apply the classifier to each element of T to detect modules and defects;
3) compare classifier's detection with the gold standard and evaluate performance metrics.

The metrics obtained are shown in Table I. Time columns represent the average time, expressed in seconds, needed to build the classifier and to perform the detection on two flight sequences.

The following consideration can be made:

- the F-measure ranges from 0,18 to 0,83 for panel detection and from 0,01 to 0,75 for defect detection;
- best results for panels and defects detection are obtained for the threshold of respectively 0.96 and 0.985; above these values, F-measure starts to decrease.
- reducing the threshold increases the Recall but quickly lowers the Precision: this can be seen more clearly in Figure 5 that reports Precision and Recall versus the threshold for Panels and Defects detection.

A. Threats to Validity and Limits of the Approach

Main error sources presented in [7] are here listed again for convenience, with the adopted remedy:

1) Payload altimeter resolution: a barometric altimeter is used to assess the RPAS altimeter resolution.

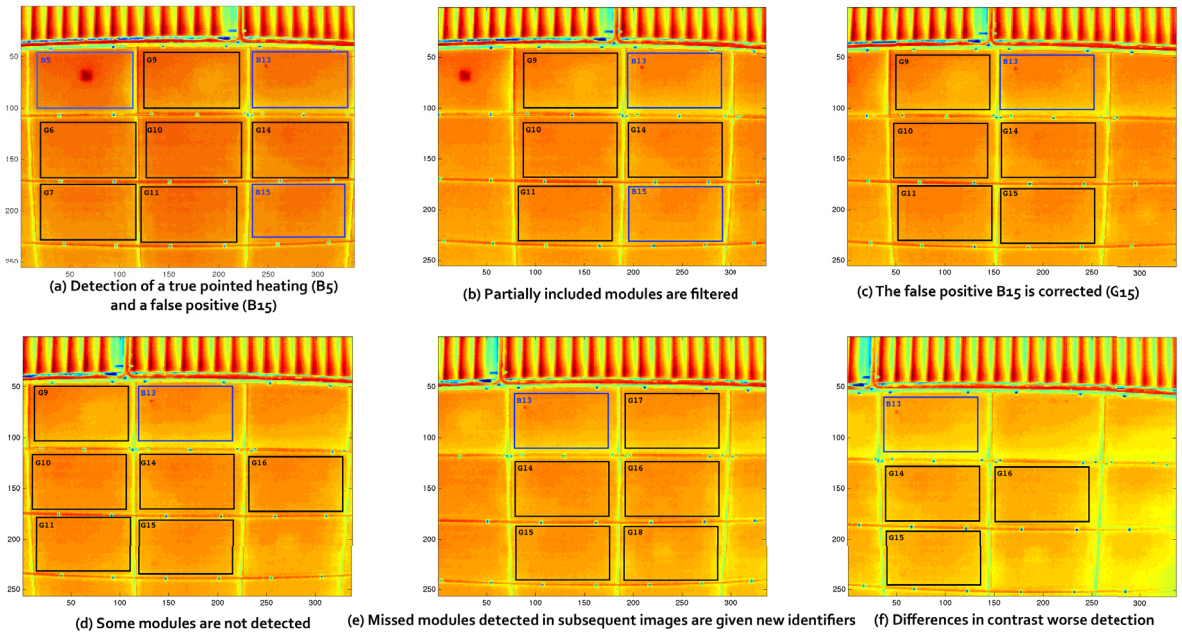

Figure 4: Panels identification and defect detection: a black boxe with a G-number ID represents an identified panel while a blue box with a B-number ID is a panel with detected defects.

		Panel Detection				Defect Detection			
Dataset	**Threshold**	**Precision**	**Recall**	**F-Measure**	**Time(sec)**	**Precision**	**Recall**	**F-Measure**	**Time(sec)**
Sequence 1 (86 images)	0,15	0,10	1,00	0,18	45s	0,00	1,00	0,01	28s
	0,25	0,13	1,00	0,22		0,01	1,00	0,01	
	0,35	0,17	0,98	0,28		0,01	1,00	0,02	
	0,45	0,25	0,95	0,40		0,02	1,00	0,03	
	0,55	0,40	0,93	0,56		0,03	1,00	0,06	
	0,65	0,46	0,93	0,61		0,06	1,00	0,11	
	0,75	0,56	0,91	0,69		0,11	1,00	0,19	
	0,85	0,63	0,89	0,74		0,60	0,75	0,67	
	0,95	0,80	0,86	0,83		0,75	0,75	0,75	
Sequence 2 (184 images)	0,15	0,10	1,00	0,18	108s	0,02	1,00	0,05	55s
	0,25	0,13	1,00	0,22		0,04	1,00	0,09	
	0,35	0,17	0,96	0,28		0,12	0,93	0,21	
	0,45	0,25	0,93	0,39		0,24	0,93	0,38	
	0,55	0,40	0,90	0,55		0,33	0,90	0,49	
	0,65	0,46	0,86	0,60		0,53	0,87	0,66	
	0,75	0,56	0,84	0,67		0,81	0,87	0,84	
	0,85	0,63	0,82	0,71		0,83	0,83	0,83	
	0,95	0,81	0,79	0,80		0,85	0,77	0,81	

Table I: Precision, Recall and F-Measure metrics for panel and defects detection, obtained for different thresholds.

2) UAV/RPAS velocity: a UAV/RPAS ground speed of typically less than 3 m/s is taken into account with respect to the GNSS receiver position update.
3) Gimbal: the orientation of gimbal must be normal to object reference system; wind gusts may introduce misalignments for few milliseconds instead; these misalignments have to be evaluated through the algorithm; typical resolutions for COTS gimbal are about 0.05°.
4) PV module Height: the height of PV panels is assessed in the case of lack of information about PV panel placement in a planar surface; this error source causes P(x;y;z0=0) not belonging to the object space.
5) PV module inclination: panels have an inclination which is typically a function of the latitude for PV plants on the ground; such inclination reduces the cross section of the panels as seen from the UAV/RPAS.
6) Sensor lens distortion: distortion is introduced by sensors optics, that have to be assessed and mitigated during the tests since they accounts for one of the most significant sources of error budget.
7) GNSS accuracy: error in position resolution obtained from the rover on-board of GNSS receiver. Further tests are needed to quantify the GNSS accuracy impact and reduce total error budget.
8) Sensor resolution: the error introduced by the commercial thermal cameras is up to 640x512 pixels.
9) Algorithm quantization: the errors introduced by the algorithm in the image reference system take into account the dimensions of the panel expressed in pixels.

A thorough assessment of the aforementioned error sources shall be done during the test and validation phases, in order to quantify the contribution of the error sources to the total subsystem error budget σ_{err}, that must always be less than the maximum error tolerance for the 95% of the time. For

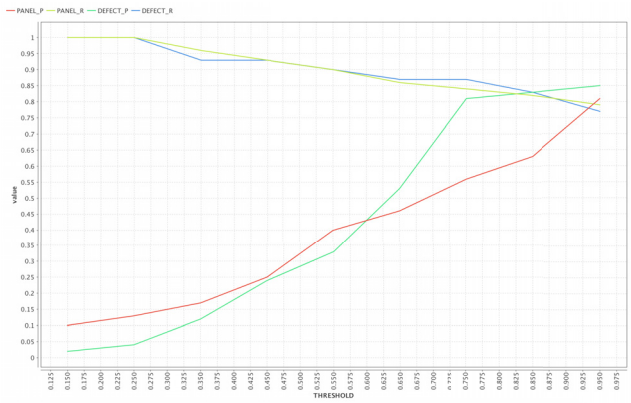

Figure 5: Precision and Recall versus Threshold for Panels and Defects Detection

the type of panels that we are considering (100cm×160cm), the subsystem error budget should be less than 50cm and the positioning error less than 20 cm. A test campaign is envisaged in the next future to validate the overall end-to-end error.

IV. Conclusions and Future Work

In this paper a computer vision approach applied to PV plant for identification and thermal anomalies detection of the panels is proposed. The approach integrates geographic information gathered from the GNSS subsystem with results of a computer vision template matching algorithm applied to thermal images (captured by the thermal camera at frequency of 1Hz). This information integration allows to perform panel identification by assigning to each module an identifier that remains consistent across different flight sessions. The template matching algorithm exploits different templates to detect both panel extension and the presence of defects. The method has been tested on different data sets on a real plant in the south of Italy and preliminary results show good performances in both panel identification (F-Measure metric = 0.80) and anomaly detection (F-Measure metric = 0.81).

As future work, the computer vision algorithm will be improved as follows:

- using both thermal and optical images;
- using RTK together with U-blox data;
- conducting a test campaign to validate the overall end-to-end error.

Furthermore the idea is to extend the algorithm validation and testing to other panels of different PV plants, by using also larger dataset to better validate the proposed approach.

Acknowledgment

The work presented in this paper is a part of the ongoing activities performed in the framework of EASY-PV project sanctioned under H2020-Galileo-2015-1 call for Small and Medium Enterprise (SME) based EGNSS application having grant agreement number 687409. The project started off on Feb. 01, 2016 and shall end on Jan. 31, 2018. The project is coordinated by Sistematica S.p.A with contributions from other partners, namely, Aalborg University, TopView srl, DeepBlue, Entec, and Alpha consultants.

References

[1] D. Feldman, D. Boff, and R. Margolis, "Q2/Q3 2016 solar industry update," *NREL, SunShot, U.S. Department of Energy*, October 2016.

[2] K. Ardani and R. Margolis, "2010 Solar Technologies Market Report," *NREL, Energy Efficiency & Renewable Energy, U.S. Department of Energy*, November 2011.

[3] P. B. Quater, F. Grimaccia, S. Leva, M. Mussetta, and M. Aghaei, "Light Unmanned Aerial Vehicles (UAVs) for Cooperative Inspection of PV Plants," *IEEE Journal of Photovoltaics*, vol. 4, no. 4, pp. 1107–1113, July 2014.

[4] C. Buerhop, R. Weißmann, H. Scheuerpflug, R. Auer, and C. J. Brabec, "Quality control of PV-modules in the field using a remote-controlled drone with an infrared camera," *Proc. of 27th Eur. Photovolt. Solar Energy Conf. Exhib., Frankfurt, Germany*, p. 3370–3373, 2012.

[5] F. Grimaccia, M. Aghaei, M. Mussetta, S. Leva, and P. B. Quater, "Planning for PV plant performance monitoring by means of unmanned aerial systems (UAS)," *Int. J. Energy Environ. Eng.*, vol. 6, no. 1, pp. 47–54, March 2015.

[6] H. Eisenbeiss, "A mini unmanned aerial vehicle (UAV): system overview and image acquisition," *Proceedings of the International Workshop on Processing and Visualization Using High-Resolution Imagery: International Archives of Photogrammetry, Remote Sensing and Spatial Information Sciences*, vol. 36-5/W1, November 2004.

[7] M. Nisi, F. Menichetti, B. Muhammad, R. Prasad, E. Cianca, A. Mennella, G. Gagliarde, and D. Marenchino, "EGNSS High Accuracy System Improving Photovoltaic Plant Maintenance using RPAS integrated with Low-cost RTK Receiver," *Proceedings of Global Wireless Summit Conference*, November 2016.

[8] B. Hofmann-Wellenhof, B. Lichtenegger, and J. Collins, *Global Positioning System*. New York: Springer-Verlag Wien, 2001.

[9] E. D. Kaplan and C. J. Hegarty, "Understanding gps: Principles and applications. second edition." 2006.

[10] D. Yoon, C. Kee, J. Seo, and B. Park, "Position accuracy improvement by implementing the DGNSS-CP algorithm in smartphones." 2016.

[11] M. Aghaei, A. Dolara, S. Leva, and F. Grimaccia, "Image resolution and defects detection in pv inspection by unmanned technologies," in *2016 IEEE Power and Energy Society General Meeting (PESGM)*, July 2016, pp. 1–5.

[12] *Performance and Reliability of Photovoltaic Systems Subtask 3.2: Review of Failures of Photovoltaic Modules*, International Energy Agency. [Online]. Available: http://iea-pvps.org/index.php?id=275&eID=dam_frontend_push&docID=2064

[13] P. Mastny, L. Radil, and Z. Mastna, "Possibilities of PV Panels Defects Identification and Determination of Its Effect on the Economy of Photovoltaic Power Plants Operation," in *Proceedings of the 2Nd International Conference on Mathematical Models for Engineering Science*, Stevens Point, Wisconsin, USA, 2011, pp. 233–238.

[14] R. Brunelli, *Template Matching Techniques in Computer Vision: Theory and Practice*. Wiley Publishing, 2009.

[15] A. Zelinsky, "Learning OpenCV–Computer Vision with the OpenCV Library (bradski, g.r. et al.; 2008)," *IEEE Robotics Automation Magazine*, vol. 16, no. 3, pp. 100–100, September 2009.

[16] A. Mahmood and S. Khan, "Correlation-coefficient-based fast template matching through partial elimination," *IEEE Transactions on Image Processing*, vol. 21, no. 4, pp. 2099–2108, April 2012.